ELSEVIER

Physics of the Earth and Planetary Interiors 130 (2002) 143–157

PHYSICS OF THE EARTH AND PLANETARY INTERIORS

www.elsevier.com/locate/pepi

A theoretical analysis of the observed variability of the geomagnetic dipole field

P. Hoyng [a,*], D. Schmitt [b,1], M.A.J.H. Ossendrijver [c]

[a] *SRON Laboratorium voor Ruimteonderzoek, Sorbonnelaan 2, 3584 CA Utrecht, The Netherlands*
[b] *Universitäts-Sternwarte, Geismarlandstraße 11, 37083 Göttingen, Germany*
[c] *Kiepenheuer Institut für Sonnenphysik, Schöneckstraße 6, 79104 Freiburg, Germany*

Received 18 July 2001; received in revised form 7 January 2002; accepted 9 January 2002

Abstract

We present a detailed analysis of the Sint-800 virtual axial dipole moment (VADM) data in terms of an $\alpha\Omega$ mean field model of the geodynamo that features a non-steady generation of poloidal from toroidal magnetic field. The result is a variable excitation of the dipole mode and the overtones, and there are occasional dipole reversals. The model permits a theoretical evaluation of the statistical properties of the dipole mode. We show that the model correctly predicts the distribution of the VADM and the autocorrelation function inferred from the Sint-800 data. The autocorrelation technique allows us to determine the turbulent diffusion time $\tau_d = R^2/\beta$ of the geodynamo. We find that τ_d is about 10–15 kyr. The model is able to reproduce the observed secular variation of the dipole mode, and the mean time between successive dipole reversals. On the other hand, the duration of a reversal is a factor $\sim$2 too long. This could be due to imperfections in the model or to unknown systematics in the Sint-800 data. The use of mean field theory is shown to be selfconsistent.

Keywords: Geodynamo; Reversals; Secular variation; Sint-800 record; Helicity fluctuations; Bistable oscillator

1. Introduction

Paleomagnetic measurements have shown that the geomagnetic field has always been approximately dipolar and aligned with the axis of rotation. The axial dipole has reversed its direction many times in the past. These reversals are fast events lasting $\lesssim 10$ kyr, and the intervals T_r between reversals have a Poisson distribution $\propto \exp(T_r/\langle T_r\rangle)$. The mean time between reversals $\langle T_r\rangle$ has decreased from $\sim 10^7$ years in the Cretaceous to about $(2\text{–}3)\times 10^5$ years during the past 10 Myr (Merrill et al., 1996; Valet and Meynadier, 1993). On shorter time scales the dipole amplitude fluctuates considerably around its mean value, see Fig. 1. This Sint-800 record of Guyodo and Valet (1999) contains detailed information on the recent behaviour of the axial dipole field, and will be analysed in this paper.

The magnetic field is generated by a dynamo located in the liquid outer core. Several groups have performed three-dimensional simulations of the complex hydromagnetic interactions involved in dynamo action (Glatzmaier and Roberts, 1995a,b; Kageyama and Sato, 1997; Kuang and Bloxham, 1997; Olson et al., 1999; Glatzmaier et al., 1999; Christensen et al., 1999). The breakthrough has come about through advances in computer technology and the low magnetic

* Corresponding author. Tel.: +31-302535600; fax: +31-302540860.
E-mail addresses: p.hoyng@sron.nl (P. Hoyng), schmitt@linmpi.mpg.de (D. Schmitt), mathieu@kis.uni-freiburg.de (M.A.J.H. Ossendrijver).
[1] Present address: Max-Planck Institut für Aeronomie, Max-Planck-Straße 2, 37191 Katlenburg-Lindau, Germany.

0031-9201/02/$ – see front matter
PII: S0031-9201(02)00004-3

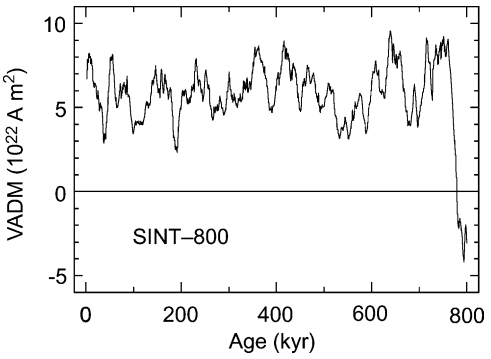

Fig. 1. The virtual akial dipole moment (VADM) of the geomagnetic field of the past 800 kiloyears, referred to as the Sint-800 record, taken from Guyodo and Valet (1999). There is one data point per 1000 yr, time is running from right to left, and we have allowed for the known reversal at $t = 780$ kyr. The errors in the individual VADM data are of the order of 10%, and the secular dipole variation dv defined in (12) is 0.071 ± 0.003.

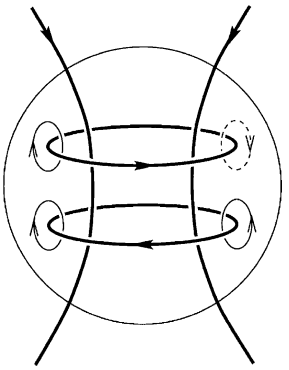

Fig. 2. We employ an $\alpha\Omega$ mean field model with a stationary fundamental mode of dipolar type (heavy lines). Differential rotation generates new poloidal field from toroidal field, and the α-effect associated with the helical convection makes new poloidal field from the toroidal field. All variability, including reversals are produced by random irregularities in the α-effect, schematically indicated by the dashed loop having the wrong orientation.

Reynolds number of the outer core. The simulations indicate that self-sustained dynamo action is able to overcome the resistive decay of the currents. And they exhibit the observed properties of the geomagnetic field: largely dipolar with $B \simeq 0.5$ G at the surface, sudden reversals and rapid variability in between. These simulations are suggestive, but unfortunately still far away from the correct parameter regime. The Ekman number, for example (ratio of viscous to Coriolis forces), is believed to be $E \sim 10^{-15}$, but the simulations can handle only $E \sim 10^{-6}$. It is therefore not clear to what extent they are representative of the geomagnetic field (see Zhang and Schubert, 2000).

Because of this and because the simulations are extremely demanding in terms of computing resources, there is a need for models that explain the dynamo process in simple physical terms, while being at the same time sufficiently rich to permit a meaningful comparison with the observations. There are many models that reproduce the observations *qualitatively* (e.g. Mazaud and Laj, 1989; Narteau et al., 2000), but a *quantitative* comparison of the predictions of models with the observed properties of the geodynamo has received little attention. The aim of the present paper is to bridge this gap.

We have developed a mean field model that is able to explain the observed statistical properties of the axial geomagnetic dipole field (Hoyng et al., 2001; Schmitt et al., 2001),[2] see Fig. 2. On general grounds we assume that the geodynamo is of the $\alpha\Omega$ type (see also Richards, 2000). We assume further that the regeneration of poloidal from toroidal magnetic field by the helical convection is non-steady on the fast eddy turnover time scale τ_c. As a result, the dynamo becomes variable, overtones are excited and there are occasional reversals. This is an old idea that goes back to Parker (1969). Because the observed distribution of the intervals between reversals is Poissonian, it seems almost unavoidable that reversals are induced by some kind of rapid variability. Parker (1969) and Levy (1972) considered a burst in helicity, immediately followed by a jump in the mean flow. Olson et al. (1983) found reversals due to jumps in the α-effect and Narteau et al. (2000) due to a steady level of helicity fluctuations.

The key elements of our model are (1) we consider a stationary level of random fluctuations in the α-effect over very long times, and (2) the statistical properties of the dipole amplitude are evaluated numerically and theoretically, with the help of a Fokker–Planck equation. This has the advantage that the physics of the model is well understood. In the present paper, we investigate how far we can bring our model to agree with the Sint-800 data. The main features of the model are

[2] Henceforth Hoyng et al. (2001) is referred to as HOS, Schmitt et al. (2001) as SOH.

summarised in Sections 2 and 3, and in the following sections we study the amplitude distribution and the autocorrelation function of the Sint-800 data.

2. Introducing the model

Our basis is the equation for the mean field (Moffatt, 1978; Krause and Rädler, 1980):

$$\frac{\partial \langle \boldsymbol{B} \rangle}{\partial t} = \nabla \times [\boldsymbol{v}x + \alpha - (\beta + \eta)\nabla \times] \langle \boldsymbol{B} \rangle. \tag{1}$$

The mean $\langle \cdot \rangle$ is interpreted as an azimuthal average, so that the mean field $\langle \boldsymbol{B} \rangle$ is the axisymmetric component of $\boldsymbol{B}$. The mean flow is written as $\boldsymbol{v} = \boldsymbol{\Omega} \times \boldsymbol{r} = \Omega r \sin\theta \, \boldsymbol{e}_\varphi$ and $\mathrm{d}\Omega/\mathrm{d}r$ is taken constant. The coefficient of turbulent diffusion β is also regarded as a constant, and much larger than the molecular resistivity η. The applicability of mean field theory to the geodynamo is discussed in Section 7. The radial dependence of the field is modeled as a spherical wave $\propto \exp(\mathrm{i}kr)/kr$, so that $1/k$ is a measure of the radial length scale of the field. This has the effect that r becomes a parameter, that we set equal to a representative radial position R. This one-dimensional model catches the dynamo action at that position R in the outer core, with crude allowance for radial turbulent diffusion. The coordinates are time t and colatitude θ. Further details may be found in HOS.

Much of the new physics of the model derives from our treatment of the dynamo coefficient α, which consists of a steady or mean part $\propto \cos\theta$ and a rapidly fluctuating part $\delta\alpha$:

$$\alpha = \alpha_\mathrm{m}(1 - q)\cos\theta + \delta\alpha(\theta, \tau). \tag{2}$$

The backreaction of the magnetic field on the flow is allowed for by taking $q \propto a_0^2$ where a_0 is the amplitude of the fundamental mode. In this way the steady part of α is a decreasing function of the energy of the fundamental mode (which is approximately the total magnetic energy). This is known as global α-quenching (Brandenburg et al., 1989).

The dynamo coefficient α is an average over the turbulent flow $\boldsymbol{u}$ superposed on $\boldsymbol{v}$. The helical convection at radial position R is assumed to consist of cells with angular size π/N_c homogeneously distributed over the sphere, $4N_\mathrm{c}^2/\pi$ in total. Each cell contributes to α a non-zero mean part $\alpha_\mathrm{m}(1 - q)\cos\theta$ and a fluctuating part $\propto fF$. The constant f gauges the strength of the fluctuations, and F is a random function of position and time with zero mean and unit variance. On taking the azimuthal average, we arrive at (2) with

$$\delta\alpha \propto \frac{fF(\theta, \tau)}{\sqrt{2N_\mathrm{c}\sin\theta}}, \tag{3}$$

since the random contribution $\propto fF$ per cell is reduced by a factor $N^{-1/2}$, where $N = 2N_\mathrm{c}\sin\theta$ is the number of cells on a circle of constant latitude, and F in (3) is updated every turnover time τ_c, independently in each latitude interval $\Delta\theta = \pi/N_\mathrm{c}$. In principle, β should also have a fluctuating part, but the fluctuations are believed to be less important for β, which is therefore regarded as a constant. Our convection model is much simpler than the model of Narteau et al. (2000). We can afford that because the emerging statistical properties of $\langle \boldsymbol{B} \rangle$ depend only very weakly on the details of the turbulence model.

We took $\delta\alpha$ to vary independently in each latitude interval because that facilitated the theoretical analysis in HOS. But this is not essential, nor is the scaling $\propto (\sin\theta)^{-1/2}$ (i.e. increasing towards the poles), or the precise functional form of the α-quenching. We argue in Section 3 that any kind of 'rapid rattling' inside the core is likely to induce a similar behaviour of variability and reversals.

The model is controlled by three parameters. Dimensionless time is defined by $\tau = t/\tau_\mathrm{d}$, i.e. time is measured in units of the turbulent diffusion time $\tau_\mathrm{d} = R^2/\beta$. In the absence of fluctuations there are two free parameters: kR and the dynamo number C_m:

$$C_\mathrm{m} = \frac{\alpha_\mathrm{m} R^4}{\beta^2}\frac{\mathrm{d}\Omega}{\mathrm{d}r}. \tag{4}$$

To simulate the geodynamo the fundamental mode of Eq. (1) must be a non-periodic dipole. This restricts the parameters to $0 < kR < 1$ and $C_\mathrm{m} > 0$. Apart from these two, the statistical properties of the model depend only on one third parameter, $f^2\tau_\mathrm{c}/N_\mathrm{c}^2$.

The applicability of our model to more general cases, for example two-dimensional models with an independent radial coordinate, requires that they also have a stationary fundamental mode. This is not immediately obvious and we defer this point to Section 7. Dynamos with a periodic fundamental mode, incidentally, react in a different way. The fluctuations generate correlated jumps in the phase and amplitude

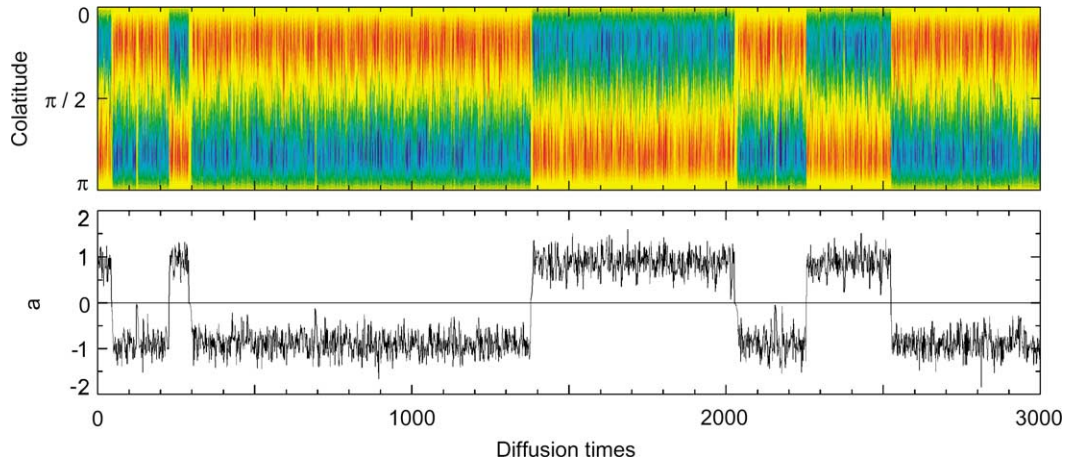

Fig. 3. Numerical solution showing the toroidal field at a representative radial position R in the outer core (top), and the normalised amplitude $a(\tau)$ of the fundamental mode (bottom). The fundamental mode is referred to as the 'dipole mode' because its poloidal field looks like an exact dipole. The dipole mode is linearly unstable for small a, the overtones are damped but transiently excited. The simulation was $5 \times 10^4 \tau_d$ long, and had 88 reversals, hence a mean reversal time $\langle T_r \rangle = 570 \pm 61$. The secular dipole variation (12) is $dv = 0.070$. This run has the same parameters as run #2 of HOS: $kR = 0.5$, $C_m = 100$, $\Lambda = 0.527$, $f^2 \tau_c / N_c^2 = 1.46 \times 10^{-2}$ ($f = 5.4$, $\tau_c = 0.05$, $N_c = 10$) and timestep $\Delta\tau = 0.01$.

of the dynamo. This has been used to explain the observed phase–amplitude correlation of the solar cycle (Ossendrijver et al., 1996; Hoyng, 1993, 1996).

3. The bistable oscillator picture

A numerical solution shows a predominantly dipolar field of varying amplitude with fine structure due to excited overtones, see Fig. 3. This run is reproduced here because it had been found to correspond closely to the Sint-800 data (cf. HOS; SOH). A major advantage of a one-dimensional model is that its properties may be conveniently determined numerically since long runs (e.g. $10^5 \tau_d$) can be performed in a short time. However, it is also possible to analyse the statistical properties of such dynamos (regardless of their dimensionality). The field is expanded in eigenmodes of the unperturbed dynamo equation at marginal excitation (eigenvalues λ^i; $\lambda^0 = 0$, Re $\lambda^i < 0$ for $i \geq 1$), and by standard techniques, we obtain [3]

$$\frac{da_i}{d\tau} = \lambda^i a_i + (1 - a_0^2) E_{ik} a_k + V_{ik}(\tau) a_k. \qquad (5)$$

[3] Summation over double *lower* indices; the factor s from HOS has been absorbed in E_{ik}.

The amplitude a_i of mode i is normalised to the amplitude a_0 of the dipole mode in non-linear equilibrium. The first term on the right gives the linear evolution, the second the supercritical excitation and the α-quenching, and the third term describes the fluctuations in α that cause all variability; E_{ik} and V_{ik} are overlap integrals of eigenmodes i and k.

By averaging the coupled mode Eq. (5) over the fluctuations the following equation can be derived for the probability distribution $p(a, \tau)$ of the amplitude a of the dipole mode:

$$\frac{\partial p}{\partial \tau} = -\frac{\partial}{\partial a} S p + \frac{1}{2} \frac{\partial^2}{\partial a^2} D p, \qquad a \equiv a_0. \qquad (6)$$

This Fokker–Planck equation is a kind of diffusion equation for the evolution of the probability distribution in terms of the drift and diffusion coefficients S and D, and it is perhaps intuitively clear that such an equation for p should exist. Presently S and D are given by

$$S \simeq \Lambda(1 - a^2)a + \text{correction term},$$
$$D \simeq \Delta_0 a^2 + \Delta_1, \qquad (7)$$

where Λ is the linear growth rate of the fundamental mode at small amplitude ($a \ll 1$). For the correction

term in (7) we refer to the Appendix A. The constants Δ_0 and Δ_1 are functions of the model parameters kR, C_m and $f^2\tau_c/N_c^2$, but the functional dependence is unfortunately unknown.

There exists a large body of literature on the Fokker–Planck equation (see Van Kampen, 1992), and this allows us to draw the following analogy. Eq. (6) is identical to the Fokker–Planck equation of a strongly damped, randomly forced particle in a bistable potential well $U(a)$ with $-\mathrm{d}U/\mathrm{d}a = S$ or, ignoring the correction term:

$$U \simeq \tfrac{1}{4}\Lambda(1-a^2)^2. \tag{8}$$

This particle-in-well paradigm is helpful to understand the physics of the geodynamo, see Fig. 4. The wells represent the normal and reversed polarity state. The particle resides in a well, performing a random motion near the bottom around the stable equilibrium, with occasional jumps to the other side (a reversal). The origin is the non-steady helical convection that amplifies the poloidal field in an irregular fashion, see Fig. 2.

The Parker–Levy reversal mechanism relies on a combination of a single cyclonic convection event, followed by a single jump in the mean flow. Provided that certain geometrical relations are satisfied a reversal may follow (Gibbons, 1998). Our model operates with a continuous level of random α fluctuations. Overtones are excited because the time scale of the fluctuations (the eddy turnover time τ_c) is much shorter than τ_d. However, most fluctuations do not result in a reversal.

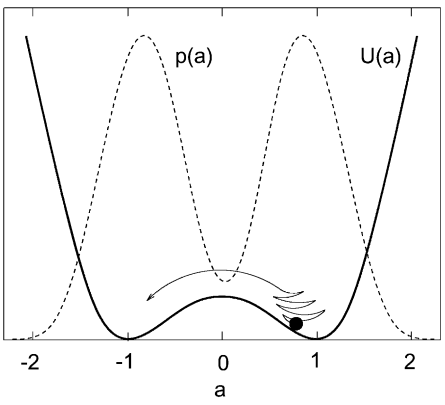

Fig. 4. The amplitude of the dipole mode behaves as the position of a randomly forced particle in a bistable potential $U(a) = (1/4)\Lambda(1-a^2)^2$. The particle is strongly damped so that the *velocity* $\mathrm{d}a/\mathrm{d}\tau$ is proportional to the force $-\mathrm{d}U/\mathrm{d}a$.

Reversals are rare because it takes a long time before *chance* produces an appropriate sequence of α fluctuations to bring about an overall sign change of the field (i.e. to push the particle to the other well in Fig. 4). In this picture reversals are a random process without a clearly identifiable cause, like radioactive decay, and analysis of a single event as in the Parker–Levy mechanism becomes meaningless. The statistical analysis of HOS yields the remarkable result that reversals must occur as soon as overtones are excited. The proof is general, and does not depend on the geometry of the overtone fields, nor on their eigenvalues, nor on the dimensionality of the dynamo. The mean reversal rate depends on an overlap integral of the poloidal field of the fundamental mode and the rms toroidal overtone field, which is reminiscent of the Parker–Levy mechanism. Since any kind of 'rapid rattling' will excite overtones, it is likely to produce reversals as well, but this has not been proven. It can further be shown that reversals are necessarily fast events lasting about a turbulent diffusion time τ_d. For details on all matters raised in this section we refer to HOS.

Eq. (6) determines all statistical properties of the dipole mode. The stationary solution is:

$$p(a) \propto \frac{1}{D}\exp\left(\int_0^a \frac{2S}{D}\,\mathrm{d}a'\right), \tag{9}$$

which reduces to

$$p(a) \propto \left(1+\frac{a^2}{c^2}\right)^{\gamma c^2+\gamma-1}\exp(-\gamma a^2), \tag{10}$$

if the correction term in (7) is ignored. This is the theoretical distribution of the dipole amplitude in its simplest form. It has two peaks near $a = \pm 1$ where most of the probability is concentrated, see Fig. 4. A better approximation to (10) is considered in the Appendix A. The parameters γ and c^2 are dimensionless measures of $U(0)$ and $D(0)$:

$$\gamma = \frac{\Lambda}{\Delta_0}, \qquad c^2 = \frac{\Delta_1}{\Delta_0}. \tag{11}$$

3.1. Status

Expression (10) is very useful as it allows us to evaluate many statistical properties of the dipole mode theoretically. So far we have studied the mean time

between reversals $\langle T_r \rangle$, and what we refer to as the 'secular dipole variation' dv:

$$dv = \frac{\langle (|a| - \langle |a| \rangle)^2 \rangle}{\langle |a| \rangle^2}, \tag{12}$$

i.e. the variance of the dipole amplitude relative to its mean value. Note that $\langle |a| \rangle = \int_0^\infty a p(a)\, \mathrm{d}a / \int_0^\infty p(a)\, \mathrm{d}a$, etc. Since the dipole mode amplitude a is proportional to the virtual axial dipole moment (VADM) within the accuracy of the Sint-800 data (Section 4.1), we can compare (10) and (12) both with the Sint-800 data and with simulation data $a(\tau)$. Other properties such as the relative fraction of time the dipole mode is below a certain threshold value, the frequency of excursions of a given magnitude, etc., may also be computed but have not yet been considered. The main results of HOS and SOH are:

(1) The Sint-800 data are well described by the theoretical distribution (10), which in turn is a reasonable approximation the numerical data $a(\tau)$. The required fluctuations are large, $\delta\alpha_{\mathrm{rms}}/\langle \alpha \rangle \sim 2.5$, and the distribution of the chron lengths (intervals between successive reversals) is Poissonian.

(2) The observations indicate a negative trend between the secular variation dv and $\langle T_r \rangle$ (McFadden and Merrill, 1995), and the model provides a simple explanation: if the forcing is increased then the particle in Fig. 4 will oscillate in the well with larger amplitude ($dv \uparrow$) but it will also jump more often to the other side ($\langle T_r \rangle \downarrow$). The value of $\langle T_r \rangle$ depends exponentially on the forcing parameter $f^2 \tau_c / N_c^2$ which is free, but also determines dv. If we require that $\langle T_r \rangle \sim 3 \times 10^5$ yrs, a typical value for the past few Myr, then $dv \simeq 0.15$, which is about the observed value in that period.

A systematic comparison of the model with the observations had not yet been undertaken. This is the subject of the following sections, where we shall investigate how far we can push the agreement between the model and the Sint-800 data, starting from the run shown in Fig. 3.

4. The distribution of the dipole amplitude

The dipole amplitude distribution of the geodynamo follows by binning the Sint-800 data. The result depends strongly on the binning method, Fig. 5. There appear to be systematic effects in the data as values around 4, 5 and $6 \times 10^{22}\,\mathrm{A\,m^2}$ seem to be overabundant. The origin of these peaks is unclear (Guyodo, private communication), but important for our work is that they are not really significant. The 1σ uncertainties e_i in each of the 799 Sint-800 data point s_i are known (Guyodo and Valet, 1999), and as a rule $e_i/s_i \sim 0.1$. Hence, the e_i are much larger than the binwidth. It follows that the 1σ uncertainty in the number of data points n_j in each bin j is roughly the Poisson value $n_j^{1/2}$. This implies a constant *relative* error of $n_j^{-1/2} = (799/50)^{-1/2} \cong 25\%$ in each individual bin level of Fig. 5, left, about as large as the peaks.

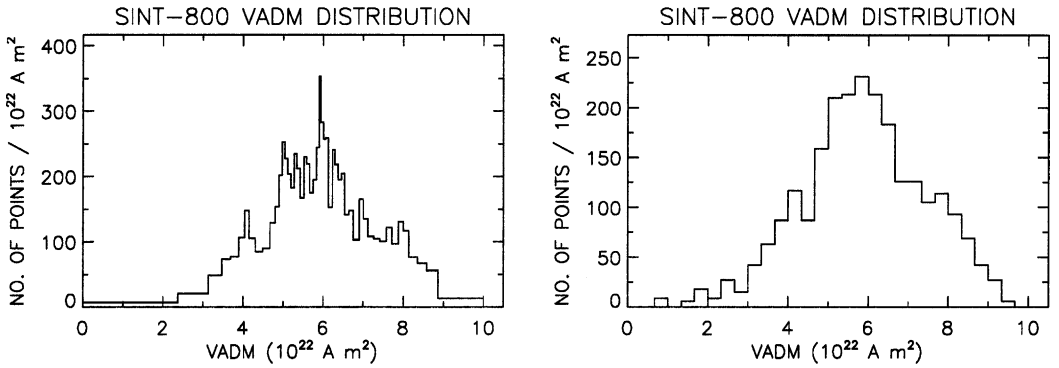

Fig. 5. The distibution of the VADM of the geodynamo according to the Sint-800 data (799 data points). Left: the data binned in 50 bins all having the same number of data points. Right: binning on a 30 point equidistant grid. The secular dipole variation dv computed from the Sint-800 data is 0.071 ± 0.003.

4.1. Fitting like to like

A few remarks on what is fitted to what are in order. The Sint-800 VADM data refer to the $\ell = 1$, $m = 0$ component of the poloidal part of the geomagnetic surface field. Each eigenmode i of Eq. (1) has a fixed spatial structure of poloidal and toroidal components which is multiplied with the time-dependent coefficient a_i. All eigenmodes have $m = 0$ (axisymmetry). The fundamental mode is antisymmetric with respect to the equator, and is called the 'dipole mode' because it has a dominant $\ell = 1$ contribution and progressively smaller $\ell = 3, 5, \ldots$ elements. The first overtone is symmetric (quadrupolar) and has only even-ℓ contributions. The second overtone is again antisymmetric (octupolar) and has still a sizable $\ell = 1$ contribution, but its mode amplitude a_2 is much smaller than a_0. It follows that the VADM is proportional to a linear combination of a_0, a_2, $a_4, \ldots$ with a dominant a_0-term. The error induced by omitting the overtones is estimated to be of the order of 10% (SOH), about as large as the error in the individual Sint-800 data. For that reason we feel justified to fit the Sint-800 data directly to a_0 (denoted as a).

The reader is alerted to the fact that we make two comparisons at the same time: one between the theoretical analysis and the model simulations (can we trust our theoretical analysis?), and one between the theoretical predictions and the Sint-800 data (does the model describe the data?). Direct fitting of simulation data to Sint-800 data is not very practical.

4.2. Optimal fit to the Sint-800 data

Fitting $p(a)$ from (10) to binned Sint-800 data proceeds as follows. Let the centroids of the bins be located at A_j, and let w_j and n_j be the width and number of data points in bin j. We choose values for the constants γ and c^2 and for the position A_m where the VADM distribution attains its maximum. Since the maximum of $p(a)$ of (10) is located at $a_\mathrm{m} = (1 - 1/\gamma)^{1/2}$, VADM values A should be rescaled as $a = (A/A_\mathrm{m})(1 - 1/\gamma)^{1/2}$. We fix the normalisation factor N of $p(a)$ by $N \sum_j p_j w_j = 799$, where p_j is the value of p at $a_j = (A_j/A_\mathrm{m})(1 - 1/\gamma)^{1/2}$. The goodness of fit is inferred from $\chi^2 = \sum_j (N p_j w_j - n_j)^2/n_j$. The procedure may then be repeated for another set of values for γ, c^2 and A_m until χ^2 reaches a minimum. To avoid problems with a small or zero number of data points n_j we use a variable binwidth as in Fig. 5 (left), and a large number of bins, typically 100. The optimal fit of (10) to the Sint-800 data thus obtained had a χ^2 corresponding to 1σ, see Table 1, case 1.

4.3. Best fit to the simulation data

The next step would be to do a simulation with the parameters just found from the fit to the Sint-800 data, but that is not as simple as it may seem. A minor problem is that two numbers (γ and c^2) is not enough to infer three model parameters kR, C_m and $f^2\tau_\mathrm{c}/N_\mathrm{c}^2$, since that could be eliminated by including additional information (e.g. on the mean time between reversals). The real snag is that we have no useful expressions for γ and c^2 in terms of the model parameters, as explained in HOS.

Since the simulation of Fig. 3 had been found to correspond closely to the Sint-800 data, we address a simpler question first: what are its values of γ and c^2? Again, there is no straightforward answer. In

Table 1
Fitting parameters

Case	Type of fit	γ	c^2	A_m (10^{22} A m^2)	χ^2 (σ)[a]	$\langle T_\mathrm{r}\rangle$[b] ($\tau_\mathrm{d}$)	dv[c]	Figure
1	(10) to Sint-800	6.3	0.32	5.98	1	1090	0.076	–
2	(10) to $a(\tau)$ of Fig. 3	8	0.50	6.07	1.3	928	0.070	–
3	(10) to both	7	0.45	6.04	1.1	665	0.079	6a
4	(A.1) to both	4.8	0.22	6.14	1.4	1097	0.071	6b
5	As 4 but $a(\tau)$ of Fig. 8	5	0.50	6.10	5	138	0.091	9

[a] Of fit of (10) or (A.1) to Sint-800 data. Quoted here and elsewhere is the value of $|\chi^2 - \nu|/(2\nu)^{1/2}$ where ν is the effective number of degrees of freedom.

[b] From relation (A.2).

[c] Computed with (12), and (10) or (A.1).

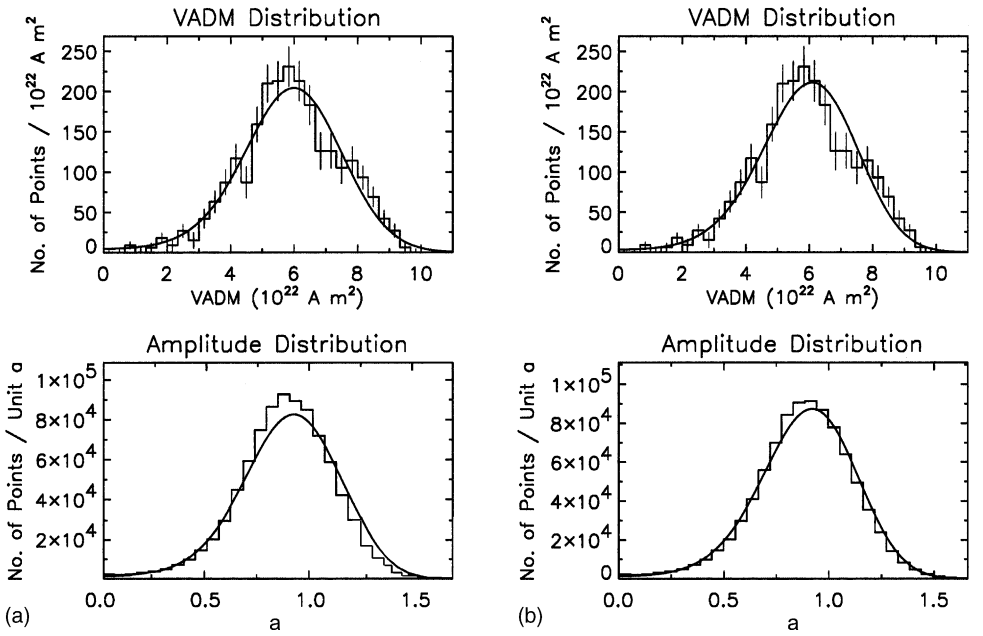

Fig. 6. (a) Left column: fit of the theoretical distribution (10) to the Sint-800 data with 1σ error bars (top panel), and to the numerical amplitudes a of Fig. 3 (bottom panel). (b) Right column: same figure, except that the improved expression (A.1) for $p(a)$ is used. In each figure (a) and (b), the horizontal axes have been scaled so that the two $p(a)$ curves coincide.

Section 5.1 of HOS an elaborate fitting method was used, but a more obvious method is to fit (10) to the numerical data $a(\tau)$. Since we know that the maximum of histogrammed numerical amplitudes a is located at $(1 - 1/\gamma)^{1/2}$ we have a two instead of the three parameter fit of Section 4.2. The result is shown in Table 1, case 2.[4] With these γ and c^2 as constraints (i.e. optimising only for A_{m} and the normalisation) we find the best fit to the Sint-800 data, which has a χ^2 corresponding to 1.3σ, see Table 1, which is quite acceptable.

Apparently, a wide range of parameter values is consistent with the Sint-800 data, among which those of Fig. 3. This suggests that the fits are insensitive to the value of γ and/or c^2, which seems surprising. In fact, the fits are quite sensitive to changes in either γ or c^2, but there is a kind of degeneracy, in that the effect of an increase in γ on the shape of $p(a)$ may be largely offset by also increasing c^2. This is visible in Table 1, cases 1–4 where c^2 is seen to increase with γ.

4.4. Compromises and improvements

Now that we have optimal fits of (10) to Sint-800 and simulation data separately, we seek a compromise to represent both. As we have just seen there is quite some leeway for that. The result is shown in Fig. 6a, and Table 1, case 3. We simply adopted the listed values of γ and c^2, in between those of the two optimal fits. Then we determine the best fit of (10) to the Sint-800 data (by adapting A_{m} and the normalisation), which had $\chi^2 \cong 1.1\sigma$ (top panel). The bottom panel compares the simulation data with (10) for these values of γ and c^2.

It is possible to improve the statistical theory by including the next correction in expression (7) for S, see Appendix A. The fit is shown in Fig. 6b and Table 1, case 4. Here, too, the values of γ and c^2 have been selected in between those of the optimal fits of (A.1) to the Sint-800 and the simulation data.

[4] The minimum χ^2 of this fit is many σ large, so that the distribution of the simulation data $a(\tau)$ deviates formally significantly from (10). The origin is that small *systematic* differences between the theory and the simulations (always present at some level) are beginning to show up, due to the fact that the fit employs so many data points (5×10^4). In that case the χ^2-test will break down.

The representation of the numerical results has improved visibly, while that of the Sint-800 data is not significantly worse ($\chi^2 \cong 1.4\sigma$).

It seems that we may conclude that the Sint-800 data, our simulations of Fig. 3 and the theory are in good agreement with one another. The theoretical values for the 'secular dipole variation' dv from Table 1 match well with the value 0.070 of the simulation of Fig. 3 and with that of the Sint-800 data, which is $dv = 0.071 \pm 0.003$. This uncertainty of 0.003 has been computed by generating sets of artificial Sint-800 data, by replacing each data point s_i by $s_i + e_i N(0, 1)$, where e_i are the known errors and $N(0, 1)$ independent draws from a normal distribution of zero mean and unit variance.

4.5. Time scales

So far we have looked only at shapes of distribution functions. We shall now consider the mean time $\langle T_r \rangle$ between reversals and the duration of reversals, and at this point a few problems appear. There is a discrepancy between the value of $\langle T_r \rangle = 570 \pm 61$ measured in the simulations of Fig. 3 and the theoretical values listed in Table 1. The latter are almost a factor 2 larger, except for the one of case 3. We impute this to the fact that relation (A.2) is only approximate, as explained in HOS. In other words, we do not regard this as a serious problem as long as we have no accurate theoretical expression for $\langle T_r \rangle$.

The question of the current value of $\langle T_r \rangle$ is trickier. There has been one reversal in the period covered by the Sint-800 data, and with that information we can only compute the 95% confidence interval: 220 kyr $< \langle T_r \rangle <$ 3.3 Myr. In HOS we concluded that $\tau_d \sim 3$ kyr so the measured value of $(570 \pm 61)\tau_d$ implies that $\langle T_r \rangle = 1.5 - 1.9$ Myr, well inside the confidence interval. This approach may seem contrived, since we may narrow down $\langle T_r \rangle$ by extending the time period: The mean reversal time was $(2–3) \times 10^5$ years in the past 10 Myr (Merrill et al., 1996; Valet and Meynadier, 1993). But for consistency it is important that the analysis of the dipole variability and the mean reversal rate refer to one and the same period, for which we have chosen the past 800 kyr of the Sint-800 data.

But there is more. The Sint-800 data actually permits us to *measure* τ_d, and the result is that τ_d is ~11 kyr rather than 3 kyr, so that $\langle T_r \rangle$ is about 6 Myr, hence outside the 95% confidence interval. We return to this issue after the next section where we illustrate how τ_d may be determined. Finally, the *duration* of a reversal is $(0.5–2)\tau_d$ in our model, which would correspond to 5–20 kyr. This is a little long but still acceptable.

5. The turbulent diffusion time of the geodynamo

The turbulent diffusion time $\tau_d = R^2/\beta$ of the geodynamo is poorly known. This is in contrast with the solar dynamo, and the reason is that the solar dynamo is periodic. In that case there are two expressions, one for the period, $P \simeq (\alpha\, \mathrm{d}\Omega/\mathrm{d}r)^{-1/2}$ in its simplest form, and one for the dynamo number (4). The period and R are known, and C_m and $\mathrm{d}\Omega/\mathrm{d}r$ are also known within the model context. Hence α, β and τ_d may be determined, at least to order of magnitude. But the geodynamo is not periodic, and only one combination of parameters (4) is known, and this renders an estimate of α and β impossible.

The idea of the method is that the curves $a(\tau)$ of Fig. 3 and the VADM of Fig. 1 are the same. After appropriate scaling of the horizontal and vertical axes one should be able to place the two on top of one another, except that the realisation of the forcing by turbulent convection is different. The appropriate tool to use under these circumstances is the autocorrelation function. The method amounts to choosing a value for τ_d to fix the absolute time axis of Fig. 3. Next, the autocorrelation function of the signal of Fig. 1 and of $a(\tau)$ are computed, and τ_d is adapted until the two curves overlap.

The expected shape of the autocorrelation function $\langle a(\tau)a(\tau + s)\rangle$ may be computed as follows. The Fokker–Planck equation (6) is equivalent to the Itô stochastic equation $\dot{a} = S + DL(\tau)$, where L is a rapidly varying Langevin force, or

$$\frac{\mathrm{d}a}{\mathrm{d}\tau} \simeq \Lambda(1 - a^2)a + DL(\tau). \tag{13}$$

(Gardiner, 1990). We are interested in small oscillations as the particle oscillates around $a = 1$ in Fig. 4, and set $a = 1 + \delta a$:

$$\frac{\mathrm{d}\delta a}{\mathrm{d}\tau} \simeq -2\Lambda\delta a + \Delta_0 L(\tau). \tag{14}$$

From this equation, the autocorrelation function of $\delta a(\tau)$ follows immediately: $\langle \delta a(\tau)\delta a(\tau + s)\rangle \propto \exp(-2\Lambda s)$, i.e. after rectifying the data to eliminate reversals and subtraction of the mean we have for this new series $\tilde{a}$ that

$$\langle \tilde{a}(\tau)\tilde{a}(\tau + s)\rangle \propto \exp(-2\Lambda s). \quad (15)$$

This approximate result says that the autocorrelation function is determined by the roll down time Λ^{-1} of the particle in the well, and that it is independent of the forcing time scale τ_c as long as $\Lambda\tau_c \ll 1$ (for the exact result see Gardiner, 1990, p. 131). This inequality is well satisfied, and hence the typical time scale of the variations that one sees in Fig. 1 is, not surprisingly, just the time scale for restoring the non-linear equilibrium of the geodynamo.

5.1. Autocorrelation functions

The autocorrelation functions in Fig. 7 have been computed as follows. The numerical data a_j (spacing $0.01\tau_d$) are processed into an artificial Sint-800 series as follows. We select a value for τ_d, rectify the data, and take a running average over τ_{av} years so that the physical time resolution corresponds to that of the Sint-800 data. Next we pick 799 consecutive points spaced by 1000 years, and subtract the mean. For the 799 Sint-800 data points s_i we reverse the direction of time and subtract the mean. For the resulting series $\{x_i\}$ we compute $\sum_{i=1}^{799-50} x_i x_{i+k}$, for $k = 0$–50, and we rescale to 1 for $k = 0$. The error bars in the Sint-800 autocorrelation of Fig. 7 are of order $799^{-1/2} \simeq 0.035$ and have been computed by generating artificial Sint-800 data, as in Section 4.4. In this way we obtain reasonable error estimates for small time shifts—in practice up to about 25 kyr.

Fig. 7a–c illustrates that the method seems to work and that τ_d can be adapted so that both autocorrelation functions overlap. Since the simulation of Fig. 3 is very long we are able to generate many sets of artificial Sint-800 data by starting at different points. The best fit for one of these other series is shown in Fig. 7f. The fit is therefore not always as good as suggested in Fig. 7b! But it is encouraging that the anticorrelation in the Sint-800 data for $t \gtrsim 25$ kyr is generally reproduced by the model. It appears that both autocorrelation functions agree best for $\tau_{av} \sim 5$ kyr and that $\tau_d \sim 10$ kyr. It is clear from Fig. 7b,d and e that $\tau_{av} = 10$ kyr is too much and $\tau_{av} = 0$ too small. This

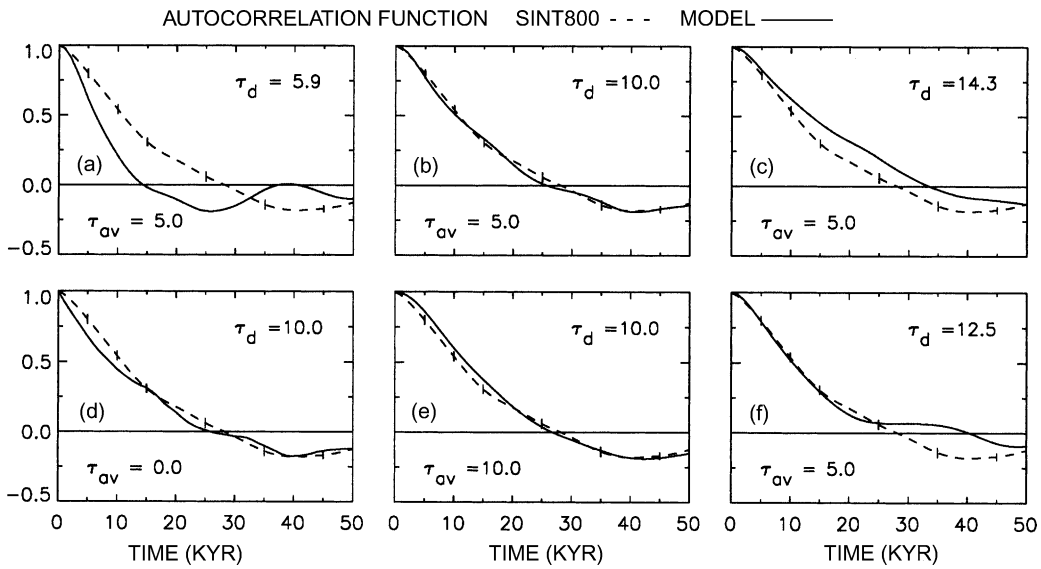

Fig. 7. Comparison of the autocorrelation functions of the Sint-800 data (dashed lines, with error bars), and of the amplitudes $a(\tau)$ of the model of Fig. 3 (drawn lines) for various choices of τ_d and τ_{av} (in kyr). The autocorrelation functions have been computed as outlined in the text. The dashed line is the same in all panels.

last autocorrelation function of Fig. 7d with $\tau_{av} = 0$ follows relation (15) quite well for small s.

After some further testing we arrived at the conclusion that the turbulent diffusion time $\tau_d = R^2/\beta = 11 \pm 2$ kyr (and that the physical time resolution of the Sint-800 data is several kyr). Like any determination of dynamo parameters, this value is model dependent. Basically we measure Λ/τ_d and Λ is model dependent.

6. Can we accomodate all constraints?

Section 4 ended with a disappointment: we had numerical data, Sint-800 data and theory all agree very closely with one another, except for the mean reversal time $\langle T_r \rangle \sim 6$ Myr, which is too large. We have explored other models with different parameters kR, C_m and $f^2\tau_c/N_c^2$ to see if it possible to reduce $\langle T_r \rangle$ while maintaining reasonable agreement in the other areas, but we have not been completely successful. Many compromises are possible and we found no clear route to an optimal model. One of the better ones is displayed in Figs. 8 and 9, and Table 1, row 5. The turbulent diffusion time determined with the autocorrelation method of the previous section is larger, $\tau_d \simeq 16 \pm 4$ kyr, mainly because the model has a larger Λ. The mean reversal time of the run in Fig. 8 was $(113 \pm 5)\tau_d$, which agrees now rather well with the theoretical value of $138\tau_d$. It would correspond to ~1.8 Myr, which lies within the confidence interval of (0.22, 3.3) Myr. The mean reversal time is smaller due to two effects, as explained in the Appendix A: $p(0)$ in Fig. 9 is larger than in Fig. 6, i.e. the amplitude a is more often near $a = 0$, and the diffusion coefficient $D \simeq \Delta_1$ is larger there.

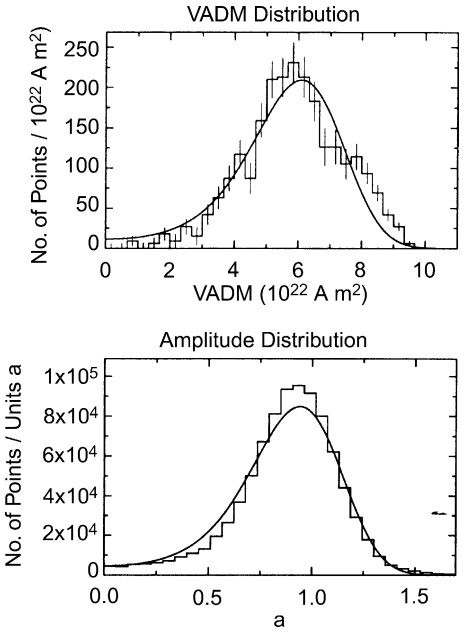

Fig. 9. Example of a fit designed to meet the criterium of a smaller $\langle T_r \rangle$. This figure is similar to Fig. 6b, and has been constructed with expression (A.1) for $p(a)$, and the numerical amplitudes a of Fig. 8.

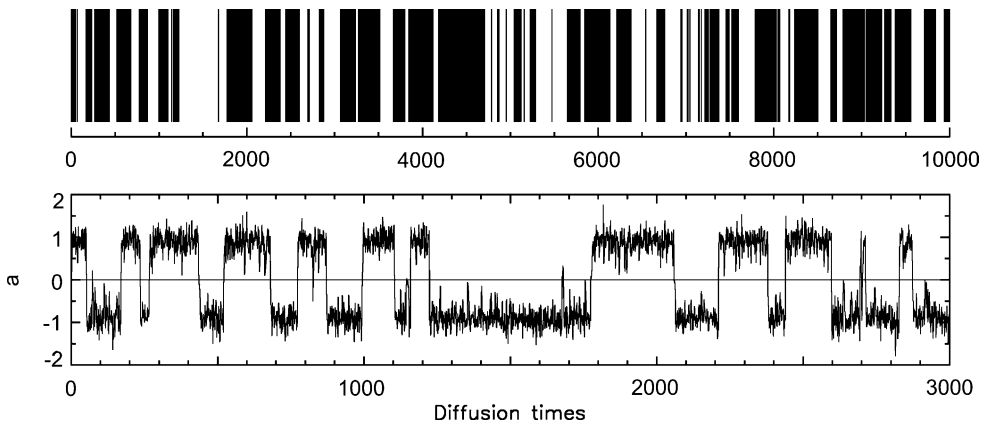

Fig. 8. Same as Fig. 3 but now for different parameters. Shown is the polarity (top), and the amplitude (bottom) of the dipole mode. The mean reversal time is 113 ± 5, and the secular dipole variation $dv = 0.081$. Parameters: $kR = 0.3$, $C_m = 120$, $\Lambda = 0.815$, $f^2\tau_c/N_c^2 = 2.45 \times 10^{-2}$ ($f = 7$, $\tau_c = 0.05$, $N_c = 10$) and timestep $\Delta\tau = 0.01$.

However, this smaller $\langle T_r \rangle$ comes at a price. The fit of (A.1) to the Sint-800 data and the simulated data in Fig. 9 is worse than in Fig. 6b. The former has a χ^2 corresponding to 5σ, see Table 1. But on the whole the fits are not unreasonable. The secular dipole variation dv of the simulation data is 0.081, somewhat larger than 0.071 ± 0.003 of the Sint-800 data. The second concern is the duration of a reversal which is now in the 8–30 kyr range, which seems to be rather long.

7. Discussion and summary

The prevailing attitude of today seems to be that only fully three-dimensional solutions of the MHD equations can provide insight in the physics of the geodynamo. Strictly speaking this is true, but there is the risk that the perspective on the basic mechanisms is lost. It may very well prove impossible to clarify the physics with simulations only. Ideally, simulations and simpler models should be developed jointly. As an example, consider Brownian motion. Although it is now feasible to follow the orbits of the many molecules colliding with the Brownian particle and with each other, the theory would be in a sorry state if one insists that only this full scale approach is meaningful, and if the simple Langevin equation that often catches much of the physics were off-limits. Against this background we have developed a mean field model for the axisymmetric component of the geomagnetic field, in particular of the dipole component. Our aim was a model that is sufficiently detailed to permit a quantitative comparison with the observations, a topic that has received surprisingly little attention. To this end we have taken into account that the regeneration of poloidal from toroidal field by the helical convection is non-steady. This is modelled by allowing for fluctuations in the dynamo parameter α on the fast eddy turnover time scale.

The model is a one-dimensional $\alpha\Omega$ dynamo and the properties of the fluctuations in the parameter α are derived from a simple picture of homogeneously distributed convection cells all having the same statistical properties. This 'minimalistic' approach suffices to account for almost all known statistical properties of the geomagnetic dipole. The fluctuations generate a variable dipole field and occasional reversals. In this picture, reversals are fast, random events without a real cause. They are rare because it takes time before the proper sequence of fluctuations materialises that is able to induce an overall sign flip. Variability and reversals are thus inseparably linked—you cannot have one without the other. Never mind how small the fluctuations and the ensuing variability, there will always be a next reversal, though the waiting time grows exponentially with the parameter $(f^2\tau_c/N_c^2)^{-1}$. This is what may have happened during the Cretaceous superchron. The model and the statistical theory that goes with it have been explained in HOS, and in this paper we have made a detailed comparison of the Sint-800 data and the model. We regard this as a first step towards a quantitative analysis of the available geomagnetic records.

Two cases have been analysed and their parameters are summarized in Table 2. We conclude that the model describes the Sint-800 data rather well, although we have not reached complete agreement. Either the mean time $\langle T_r \rangle$ between reversals (case 1) or the duration of a reversal is too long (case 2). The difficulty may be traced back to the value of the turbulent diffusion time $\tau_d = R^2/\beta$. If that had been a factor 2–3 times smaller the model would describe the data perfectly. This may indicate that our model is not adequate. However, we may also have overlooked certain effects while constructing the artificial Sint-800 series. We did allow

Table 2
Model parameters

Case	Figure	kR	C_m	$f^2\tau_c/N_c^2$	τ_d (kyr)	τ_r (kyr)[a]	$\langle T_r \rangle$[b] (Myr)	dv[c]	β/η
1	3, 6b	0.5	100	1.46×10^{-2}	11 ± 2	5–20	5–7.5	0.070	~30
2	8, 9	0.3	120	2.45×10^{-2}	16 ± 4	8–30	1.3–2.2	0.081	~ 20

[a] Duration of a reversal.
[b] From run, and the value of τ_d.
[c] From run; the Sint-800 value is 0.071 ± 0.003.

for the finite physical time resolution of the Sint-800 data by taking a running average, but there may be other, systematic effects (see for example, Section 4). We have not used the data of Valet and Meynadier (1993) which comprise a period of 4 Myr, because they are less reliable than the Sint-800 data. But it may be worthwhile to apply our analysis to these data as well because the mean time between reversals would be much better constrained. Taking all things together we think our results look promising, given that this is only the first time an analysis of this type has been undertaken. For the same reason we did not employ any of the more advanced (maximum likelihood) fitting methods which have the advantage that binning is no longer necessary, but require a considerably larger computational effort.

We now address the question whether our results will carry over to more realistic two-dimensional models with an independent radial coordinate. The answer is affirmative, provided the model has a stationary fundamental dipole mode. Briefly, the reason is that the mode equations (5), the starting point of the analysis, do not depend on the dimensionality of the dynamo (for details see HOS). It is true that classical $\alpha\Omega$ dynamos in a two-dimensional sphere or spherical shell tend to have oscillatory solutions (Roberts, 1972), but several mechanisms have been proposed that favour stationary dynamo action. One is spatial separation of the induction effects (Deinzer et al., 1974; Gibbons, 1998). Furthermore, α^2 dynamos are usually non-oscillatory (Roberts, 1972). Meridional circulation is another mechanism known to promote stationary dynamo action (Roberts, 1972; Sarson and Jones, 1999). Finally, a conducting solid inner core inhibits oscillatory dynamo action and has a stabilising effect (Hollerbach and Jones, 1993; Glatzmaier and Roberts, 1995a,b). We are confident that there exists a range of realistic two-dimensional models with a stationary fundamental dipole mode. We have constructed a model with a passive conducting inner core and the initial tests look promising.

Such a model would allow us for example to study the influence of the inner core, and to address the question whether the duration of a reversal is set by the Ohmic diffusion time of the inner core as suggested by Gubbins (1999), or by the turbulent diffusion time τ_d of the outer core as in the present model. From our experience with the work of Section 6, we expect that most models with a stationary fundamental mode can be tuned to reproduce the statistical properties of the geomagnetic dipole field. The models without fluctuations serve as a 'substrate' generating the bistable potential of Fig. 4. By fitting the data as in the present paper, we shall be able to determine some characteristics of the bistable potential such as slopes and the height of the central hill. Trade-offs are possible, where a change in one parameter is compensated by changing another. Hence we shall gain only a limited amount of information on the 'substrate model'. But a wholly succesful fit to the data and a more reliable set of fluctuation parameters may be in the offing. This in turn will enhance confidence in rapid (helicity) fluctuations as a generic mechanism for inducing variability and reversals.

Finally, our acceptance of mean field theory to describe the physics of the geodynamo needs clarification. It is true that geodynamo theory could afford to move away from mean field theory, due to the low magnetic Reynolds number of the outer core, but the question whether or not mean field theory applies has never really been settled. A decisive issue is the value of the eddy magnetic Reynolds number $R_\mathrm{m} = u\lambda_\mathrm{c}/\eta \sim \beta/\eta$ (since $u\tau_\mathrm{c} \sim \lambda_\mathrm{c}$). We infer β from $\beta = R^2/\tau_\mathrm{d}$ and $R = 3500\,\mathrm{km}$. The conductivity of the core is $6 \times 10^5\,\mathrm{S\,m^{-1}}$ (Merrill et al., 1996, p. 274) whence $\eta \sim 1.3 \times 10^4\ \mathrm{cm^2\,s^{-1}}$. The resulting eddy magnetic Reynolds numbers β/η are perhaps just large enough to support the notion of field lines frozen into the eddy convection. We infer from (4) that $\alpha_\mathrm{m}\Omega' = C_\mathrm{m}/\tau_\mathrm{d}^2$, and take $\Omega' = \mathrm{d}\Omega/\mathrm{d}r \simeq -2.4\times10^{-18}\,(\mathrm{cm\,s})^{-1}$, corresponding to a differential rotation of -1° per years over $\Delta R = 2300\,\mathrm{km}$, the depth of the outer core (Richards, 2000). This leads to $\alpha_\mathrm{m} \sim -2.5 \times 10^{-4}\,\mathrm{cm\,s^{-1}}$. Next $C_\alpha \equiv \alpha_\mathrm{m}R/\beta$ and $C_\Omega \equiv \Omega' R^3/\beta$ may be computed to find that $C_\alpha/C_\Omega \sim 10^{-3}$, so that the $\alpha\Omega$ approximation is justified.

Acknowledgements

We acknowledge an extensive correspondence with Dr. Y. Guyodo, as well as discussions with Prof. R.D. Gill and Prof. C.G. Langereis. During the initial stages of the data analysis we have benefitted from the help of Mr. E.M.W.P. Haverkamp.

Appendix A. Improved expression for $p(a)$

A more accurate expression for $p(a)$ can be obtained by allowing for the correction term in the definition (7) of S. This correction has been considered in Appendix B.1 of HOS. To reduce the technicalities to a minimum we jump now to the end of that Appendix where the function $g_1(a)$ is derived. We also adopt temporarily the notation used there without further introduction. It was argued there that $g_1(a)$ is of the form $g_1(a)/(1-a^2) = Aa(1+Ba^2+\cdots)$. In HOS only the term Aa was included, and then relation (HOS, 33) says that $S = \mu(1-a^2)a + A(1-a^2)a = \Lambda(1-a^2)a$. To be able to include the next term ABa^3 we require the value of B.

Comparing the expression $g_1(a)/(1-a^2) = Aa(1+Ba^2+\cdots)$ with relation (HOS, B3) we find that $Aa(1+Ba^2) \propto \int_0^\pi \mathrm{d}\theta\, \sin\theta\cos\theta\, \tilde{P}_0\, \langle T_+\rangle|_a$. We have computed $\langle T_+\rangle|_{a=1}$ numerically, by storing the function $T_+(\theta)$ each time a passes through 1 during the simulation of Fig. 3, and find that $\langle T_+\rangle|_{a=1} = 0$ to good approximation. Intuitively, this is a reasonable result: when the amplitude of the dipole mode is equal to its value in the non-linear equilibrium, the overtone amplitudes are apparently zero on average. It follows that $Aa(1+Ba^2+\cdots)$ must be zero in $a=1$, or $B=-1$ if we ignore the higher-order terms. This leads to $S = \Lambda(1-a^2)a + (\mu-\Lambda)(1-a^2)a^3$. After insertion in (9) and some algebra we obtain:

$$p(a) \propto \frac{1}{a^2+c^2} \times \exp\left\{\gamma \int_0^{a^2} \frac{1+(\mu/\Lambda-1)x}{x+c^2}(1-x)\,\mathrm{d}x\right\}. \tag{A.1}$$

Here, γ and c^2 are defined as in (11) and the value of μ/Λ is known for a given model (1.45 for Fig. 3, and 1.82 for Fig. 8). The correction term in S can still be recognised as the factor $(\mu/\Lambda - 1)$ in the numerator of (A.1), and if it is set equal to zero one regains (10). Explicit evaluation of (A.1) is straightforward but suppressed here. Since the highest-order term in the integrand is $\propto x$, the exponent now contains an a^4-term. The maximum a_m of (A.1) where $p'(a) = 0$ turns out to follow from a simple quadratic equation, $\{1+(\mu/\Lambda - 1)a_\mathrm{m}^2\}(1-a_\mathrm{m}^2) = 1/\gamma$ (and if $\mu/\Lambda - 1$ is set to zero again, we get $a_\mathrm{m} = (1-1/\gamma)^{1/2}$ as mentioned in Section 4.2). The expression for $\langle T_\mathrm{r}\rangle$ is

$$\langle T_\mathrm{r}\rangle \approx \frac{4\pi}{\Delta_1}\left(\frac{1}{\phi_0''\psi_\mathrm{m}''}\right)^{1/2}\exp(\psi_\mathrm{m}) = \frac{4\pi}{\Delta_1}\left(\frac{1}{\phi_0''\psi_\mathrm{m}''}\right)^{1/2}\frac{p(a_\mathrm{m})}{p(0)}. \tag{A.2}$$

For the definition of the functions $\psi(a)$ and $\phi(a)$ we refer to Appendix A of HOS; $\phi_0'' = \phi''(0)$, and ψ_m, ψ_m'' are the value of ψ and ψ'' in $a = a_\mathrm{m}$. The first expression in (A.2) has been given in Appendix F of HOS, and the second follows because $p(a) \propto \exp[\psi(a)]$ and $\psi(0) = 0$. The functions $\psi(a)$ and $\phi(a)$ become more complicated when the correction term in the definition (7) of S is included, but relation (A.2) remains valid as it stands. We have derived explicit expressions for $\langle T_\mathrm{r}\rangle$ from (A.2), as well as for dv. These expressions are needed for the computations described in the text, but details are omitted here.

The second relation in (A.2) is given here because it demonstrates that $\langle T_\mathrm{r}\rangle$ is particularly sensitive to the values of $p(0)$ and of the diffusion coefficient Δ_1 in $a = 0$, because ϕ_0'', ψ_m'' and $p(a_\mathrm{m})$ are rather well determined by the fitting procedure.

References

Brandenburg, A., Krause, F., Meinel, R., Moss, D., Tuominen, I., 1989. The stability of non-linear dynamos and the limited role of kinematic growth rates. Astronom. Astrophys. 213, 411–422.

Christensen, U., Olson, P., Glatzmaier, G.A., 1999. Numerical modelling of the geodynamo: a systematic parameter study. Geophys. J. Int. 138, 393–409.

Deinzer, W., Von Kusserow, H.-U., Stix, M., 1974. Steady and Oscillatory $\alpha\omega$-dynamos. Astronom. Astrophys. 36, 69–78.

Gardiner, C.W., 1990. Handbook of Stochastic Methods. Springer, Berlin.

Gibbons, S.J., 1998. The Parker–Levy reversal mechanism. Phys. Earth Planet. Inter. 106, 129–137.

Glatzmaier, G.A., Roberts, P.H., 1995a. A three-dimensional self-consistent computer simulation of a geomagnetic field reversal. Nature 377, 203–209.

Glatzmaier, G.A., Roberts, P.H., 1995b. A three-dimensional convective dynamo solution with rotating and finitely conducting inner core and mantle. Phys. Earth Planet. Inter. 91, 63–75.

Glatzmaier, G.A., Coe, R.S., Hongre, L., Roberts, P.H., 1999. The role of the Earth's mantle in controlling the frequency of geomagnetic reversals. Nature 401, 885–890.

Gubbins, D., 1999. The distinction between geomagnetic excursions and reversals. Geophys. J. Int. 137, F1–F3.

Guyodo, Y., Valet, J.-P., 1999. Global changes in intensity of the Earth's magnetic field during the past 800 kyr. Nature 399, 249–252.

Hollerbach, R., Jones, C.A., 1993. Influence of the Earth's inner core on geomagnetic fluctuations and reversals. Nature 365, 541–543.

Hoyng, P., 1993. Helicity fluctuations in mean field theory: an explanation for the variability of the solar cycle? Astronom. Astrophys. 272, 321–339.

Hoyng, P., 1996. Is the solar cycle timed by a clock? Sol. Phys. 169, 253–264.

Hoyng, P., Ossendrijver, M.A.J.H., Schmitt, D., 2001. The geodynamo as a bistable oscillator. Geophys. Astrophys. Fluid Dynamics 94, 263–314 (HOS).

Kageyama, A., Sato, T., 1997. Generation mechanism of a dipole field by a magnetohydrodynamic dynamo. Phys. Rev. E 55, 4617–4626.

Krause, F., Rädler, K.-H., 1980. Mean Field Magnetohydrodynamics and Dynamo Theory. Akademie Verlag, Berlin.

Kuang, W., Bloxham, J., 1997. An Earth-like numerical dynamo model. Nature 389, 371–374.

Levy, E.H., 1972. Kinematic reversal schemes for the geomagnetic dipole. Astrophys. J. 171, 635–642.

Mazaud, A., Laj, C., 1989. Simulation of geomagnetic polarity reversals by a model of interacting dipole sources. Earth Planet. Sci. Lett. 92, 299–306.

Merrill, R.T., McElhinny, M.W., McFadden, P.L., 1996. The Magnetic Field of the Earth. Academic Press, New York.

Moffatt, H.K., 1978. Magnetic Field Generation in Electrically Conducting Fluids. Cambridge University Press, Cambridge.

Narteau, C., Blanter, E., Le Mouël, J.-L., Shirnman, M., Allègre, C.J., 2000. Reversal sequence in a multiple scale dynamo mechanism. Phys. Earth Planet. Inter. 120, 271–287.

Olson, P., 1983. Geomagnetic polarity reversals in a turbulent core. Phys. Earth Planet Inter. 33, 260–274.

Olson, P., Christensen, U., Glatzmaier, G.A., 1999. Numerical modeling of the geodynamo: Mechanisms of field generation and equilibration. J. Geophys. Res. 104, 10383–10404.

Ossendrijver, A.J.H., Hoyng, P., Schmitt, D., 1996. Stochastic excitation and memory of the solar dynamo. Astronom. Astrophys. 313, 938–948.

Parker, E.N., 1969. The occasional reversal of the geomagnetic field. Astrophys. J. 158, 815–827.

Richards, P.G., 2000. Earth's inner core—discoveries and conjectures. Astronom. Geophys. 41, 1.20–1.24.

Roberts, P.H., 1972. Kinematic dynamo models. Philos. Trans. R. Soc. A272, 663–698.

Sarson, G.R., Jones, C.A., 1999. A convection driven geodynamo reversal model. Phys. Earth Planet. Inter. 111, 3–20.

Schmitt, D., Ossendrijver, M.A.J.H., Hoyng, P., 2001. Magnetic field reversals and secular variation in a bistable geodynamo model. Phys. Earth Planet. Inter. 125, 119–124 (SOH).

Valet, J.-P., Meynadier, L., 1993. Geomagnetic field intensity and reversals during the past four million years. Nature 366, 234–238.

Van Kampen, N.G., 1992. Stochastic Processes in Physics and Chemistry. North-Holland, Amsterdam.

Zhang, K., Schubert, G., 2000. Magnetohydrodynamics in rapidly rotating spherical systems. Annu. Rev. Fluid Mech. 32, 409–443.